



## Biological activity of Eudragit loaded $\text{Eu}_2\text{O}_3$ , and $\text{WO}_3$ nanocomposites against *Staphylococcus* and *Streptococcus* strains

Geeta, Pallavi Bhardwaj and Sunil K. Jangra

Research Scholar, Baba Mastnath University, Asthal Bohar, Rohtak, Haryana  
Associate Professor, Baba Mastnath University, Asthal Bohar, Rohtak, Haryana  
Assistant Professor, AIJHM College, Rohtak, Haryana

### ABSTRACT

The synthesis of nanocomposites consisting of Eudragit,  $\text{Eu}_2\text{O}_3$  (Europium trioxide), and  $\text{WO}_3$  (Tungsten (VI) Oxide) was conducted utilizing the emulsion solvent evaporation process. The concentrations of Eudragit,  $\text{Eu}_2\text{O}_3$ , and  $\text{WO}_3$  were systematically varied during the synthesis. The experimental characterization of the EWENPs included assessments of their drug encapsulation efficiency, power for prospective drug encapsulation, particle size distribution, shape of nanoparticles, zeta potential for stability, Fourier-transform infrared spectroscopy (FTIR) analysis, and evaluations of drug release rate. The *in vitro* antioxidant activity and anti-inflammatory efficacy of  $\text{Eu}_2\text{O}_3$  and  $\text{WO}_3$  were assessed using an analysis of their release profiles. The experimental results indicated that the size of EWENPs fell within the range of 119-284 nm while exhibiting a high encapsulation efficiency of 89-92%. In addition, nanoparticles were successfully synthesized using Eudragit at a concentration of 0.4 mg/ml and DMSO (1 ml). These nanoparticles were characterized as isolated and free-flowing. Subsequently, the antibacterial properties of these nanocomposites were evaluated, revealing their effectiveness against *Staphylococcus* and *Streptococcus* strains.

**Keywords:** Eudragit,  $\text{Eu}_2\text{O}_3$ ,  $\text{WO}_3$ , Nanocomposites, Anti-bacterial.

Received 20.12.2023

Revised 15.01.2023

Accepted 13.02.2024

### INTRODUCTION

In recent decades, there have been advancements in the development of new materials, specifically nanopowders, nanocomposites, and nanofibers, which possess dimensions of less than 100 nm in at least one direction [1]. Nanocomposites exhibit distinctive biological features as a result of their quantum size and a notable augmentation in the ratio of surface atoms to bulk materials [2]. Specifically, the antibacterial capabilities exhibited by these substances render them suitable for utilization in a wide range of human and industrial contexts [3]. The antibacterial properties of nanoparticles (NPs) are attributed to their ability to penetrate, small size, chemical toxicity, and capacity to disrupt the bacterial cell membrane and generate reactive oxygen species (considered the principal mode of action) [4]. Previous research has demonstrated that the antimicrobial properties are attributed to the presence of metal in cationic form, rather than metallic form [5]. Nanofilms composed of metallic ions and polymers have been employed as nanocomposites for wound coverage, specifically targeting infections produced by *Staphylococcus aureus* and *Pseudomonas aeruginosa* [6]. The synthesis of polymer-metal oxide nanocomposites is a burgeoning area of research, driven by its potential technological applications in various fields including rechargeable batteries, fuel cells, and supercapacitors [6]. Eudragit is a commonly encountered conducting polymer that has received relatively limited attention within the realm of polymer nanocomposite research [7].

The qualities of eudragit, including photoluminescence, thermal stability, high redox potential, and optical characteristics, have garnered significant attention from researchers in the field of nanocomposites—the utilization of eudragit nanocomposites in the domains of optoelectronics, anti-cancer and gas sensors [8]. Eudragit S100 polymers have been extensively investigated as pH-responsive polymers for the oral administration of small drugs. Eudragit is a commercially available acrylate compound that exhibits pH sensitivity, making it suitable for use in the enteric coating of tablets and capsules. These polymers facilitate the functionality of the active ingredient in your solid dose form as it traverses the gastrointestinal tract.

The ability to effectively blend several polymers allows for the attainment of the intended drug release profile, ensuring precise drug release at the appropriate location and timing, and perhaps extending the duration of release as needed. Additional crucial tasks include safeguarding against external factors such

as moisture, as well as enhancing patient adherence through the concealment of flavor or odor [9]. Our product line offers a wide range of options that allow for flexibility in achieving tailored medication release profiles [10]. These options include enteric, protective, and sustained-release features, all of which are designed to give optimal performance. EUDRAGIT® polymers are copolymers that are synthesized from esters of acrylic and methacrylic acid. The physicochemical properties of these polymers are influenced by the presence of functional groups denoted as R. EUDRAGIT® polymers are offered in many physical forms, including aqueous dispersions, organic solutions, granules, and powders. A differentiation is established between poly(meth)acrylates, which possess solubility in digestive fluids through the process of salt production [11]. The EUDRAGIT® L, S, FS, and E polymers possess acidic or alkaline groups, which facilitate the release of the active component in a pH-dependent manner. Metal and metal oxide nanoparticles doped polymer nanocomposites have demonstrated significant antibacterial properties [12].  $\text{Eu}_2\text{O}_3$  and  $\text{WO}_3$  are considered to be highly significant metals in the production of polymer nanocomposites that exhibit improved antibacterial properties. The potential of antioxidants in the realm of medicine has been investigated and substances with antibacterial properties [12].

The activities of  $\text{Eu}_2\text{O}_3$  and  $\text{WO}_3$  nanoparticles that possess can eliminate several bacterial infections<sup>13</sup>. Nanotechnology-based  $\text{Eu}_2\text{O}_3$  and  $\text{WO}_3$  are characterized by their non-toxic properties used as a secure and effective antibacterial agent for the human body [14]. There is a prevailing belief that  $\text{Eu}_2\text{O}_3$  and  $\text{WO}_3$  engage in interactions with sulfur, oxygen, and nitrogen present in microbe molecules, hence leading to the deactivation of cellular proteins and ultimately resulting in cell demise [1]. The efficacy and minimal cytotoxicity of  $\text{Eu}_2\text{O}_3$  and  $\text{WO}_3$  towards animal cells. The present study investigates the antibacterial properties of eudragit-loaded  $\text{Eu}_2\text{O}_3$  and  $\text{WO}_3$  nanocomposites against *Staphylococcus* and *Streptococcus* stains

## **MATERIAL AND METHODS**

### **Materials**

The eudragit used in this study was obtained from Hi-Media Pvt. Ltd., located in Mumbai, India.  $\text{Eu}_2\text{O}_3$  and  $\text{WO}_3$  were procured from Sigma Aldrich, India, while Minimum Essential Eagle Medium, Foetal bovine serum (FBS), and penicillin & streptomycin antibiotics were acquired from Himedia Laboratories Pvt. Ltd. Mumbai, India. All compounds utilized in the current study were of analytical reagent grade.

### **Preparation of $\text{Eu}_2\text{O}_3$ and $\text{WO}_3$ loaded Eudragit nanoparticles (EWENPs)**

The polymeric nanoparticles of  $\text{Eu}_2\text{O}_3$  and  $\text{WO}_3$  were produced using the emulsion solvent evaporation process. A mixture was prepared by combining 5 mg of  $\text{Eu}_2\text{O}_3$  and 5 mg of  $\text{WO}_3$  in 10 ml of methanol. In a separate step, Eudragit was dissolved in distilled water at a concentration range of 0.01-0.10 grams. A solution containing  $\text{Eu}_2\text{O}_3$  and  $\text{WO}_3$  was added dropwise to a eudragit solution while being stirred at 500rpm using a magnetic stirrer for 30 minutes. The mixture of  $\text{Eu}_2\text{O}_3$  and  $\text{WO}_3$ -eudragit was gradually introduced into the aqueous phase, namely a 1-2ml solution of DMSO in water. The resulting solution was subjected to magnetic stirring at a rate of 500 revolutions per minute for 18 hours or overnight. Following the successful attainment of full solubility of  $\text{Eu}_2\text{O}_3$ ,  $\text{WO}_3$ , and eudragit, organic phase solutions were employed. The methanol component of the organic phase underwent complete evaporation and subsequent centrifugation at a speed of 10000 revolutions per minute at a temperature of 4 degrees Celsius for a duration of 40 minutes. The liquid portion was collected and subjected to analysis using a UV spectrophotometer to determine the presence of unbound  $\text{Eu}_2\text{O}_3$  and  $\text{WO}_3$  molecules. The produced EWENPs were further subjected to separation, followed by two rinses with double distilled water and subsequent lyophilization [16].

### **In vitro release profile of EWENPs**

The dialysis sac method was employed to investigate the release patterns of  $\text{Eu}_2\text{O}_3$  and  $\text{WO}_3$ . The  $\text{Eu}_2\text{O}_3$  and  $\text{WO}_3$  (5 mg) entrapped eudragit-loaded nanocomposites were placed within a dialysis sac and subsequently submerged in a standard phosphate buffer solution (0.1 M) with a pH of 7.4. The solution was continuously swirled at a rate of 120 revolutions per minute, maintaining a constant temperature of 27°C. A 2-milliliter sample was extracted and gathered at consistent intervals of 1, 2, 3, 6, 12, and 24 hours. The absorbance of the samples was then assessed using a UV spectrophotometer set at a wavelength of 414 nanometres [17].

### **Characterization of synthesized EWENPs**

The Zetasizer Nano ZS-90 instrument was utilized to determine the mean size range and size distribution of nanoparticles. The quantity of unbound  $\text{Eu}_2\text{O}_3$  and  $\text{WO}_3$  in the supernatant, acquired after high-speed centrifugation at 10000 rpm and 4°C for 45 minutes, was determined using a UV spectrophotometer. Subsequently, the percentage encapsulation efficiency was estimated using the following formula:

The term "percentage" refers to a numerical representation of a proportion or fraction expressed as a The entrapment efficiency can be calculated by multiplying the ratio of unbound drug to total drug by 100.

The morphology of extracellular water-extracted nanoparticles (EWENPs) was analyzed using a transmission electron microscope (TEM: Hitachi H7500). The nanoparticles were deposited onto a copper grid and imaged using a transmission electron microscope (TEM) at a magnification of 60,000x and an accelerating voltage of 80,000V. The scanning electron microscope (SEM) is capable of generating high-resolution images of individual nanoparticles with dimensions significantly less than 10 nm [18]. Atomic force microscopy (AFM) possesses an exceptional capacity for high-resolution imaging, with a demonstrated resolution capability that surpasses the optical diffraction limit by a factor of 1200. The Fourier transform infrared (FTIR) analysis of Eu<sub>2</sub>O<sub>3</sub>, WO<sub>3</sub>, eudragit, and EWENPs was conducted using an FTIR Affinity-1 spectrophotometer (Shimadzu, Japan) within the wave number range of 4500–500 cm<sup>-1</sup>.

#### **Antioxidant activity**

The antioxidant capacity of Eu<sub>2</sub>O<sub>3</sub>, WO<sub>3</sub>, eudragit, and EWENPs was assessed using the DPPH assay. The compound 1,1-diphenyl-2-picrylhydrazyl (DPPH), which serves as a free radical intermediate, was solubilized in methanol at a standard concentration of 4mg per 100 ml. To investigate the inhibition of DPPH, the pure Eu<sub>2</sub>O<sub>3</sub>, WO<sub>3</sub>, eudragit, and EWENPs were subjected to incubation with DPPH for 25 minutes under complete darkness. The resulting absorbance was then measured using a UV spectrophotometer at a wavelength of 517 nm<sup>19</sup>. This analysis was performed in triplicate, as stated in the reference. Blank Eudragit nanoparticles (NPs) were utilized as a control group with no active components, whereas pure Eu<sub>2</sub>O<sub>3</sub> and WO<sub>3</sub> were employed as the experimental groups with known favorable effects [20].

Percent antioxidant activity =  $\frac{\text{Absorbance of control} - \text{Absorbance of sample}}{\text{Absorbance of control}} \times 100$

Absorbance of control

#### **Anti-Inflammatory Activity**

The anti-inflammatory properties of EWENPs were assessed using the HRBC membrane stabilization technique across a range of doses, namely from 0.100 to 0.400 mg/ml. A blood sample was obtained from a healthy individual and subjected to centrifugation at a speed of 3000 revolutions per minute for 10 minutes. The resulting packed cells were then collected using a micropipette. The procedure was iterated two to three times until a distinct supernatant was acquired [21]. A mixture for the assay was created by combining 1 ml of samples with varying concentrations, 1 ml of phosphate buffer, and 2 ml of hyposaline solution. This mixture was then combined with 0.5 ml of HRBCs. In the experiment, the control group was administered distilled water instead of hyposaline [22].

## **RESULTS AND DISCUSSION**

### **Particle size and Zeta potential**

The size and zeta (stability) potential of EWENPs were assessed by the utilization of dynamic light scattering techniques. The size of the optimized nanocomposite was determined to be 124.5 nm, as illustrated in Figure 1. The zeta potential of EWENPs is measured to be -45.1 mV, as shown in Figure 2. This value indicates the stability of the nanoformulations<sup>23</sup>.

**Figure 1. PSA image of EWENPs**

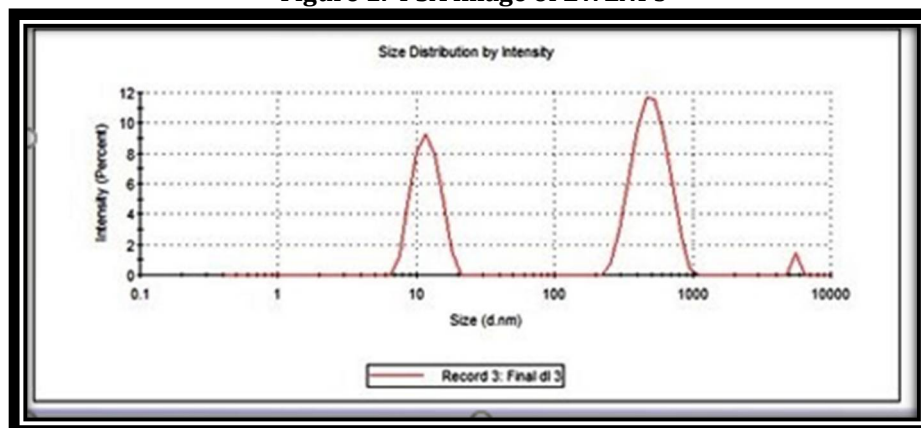
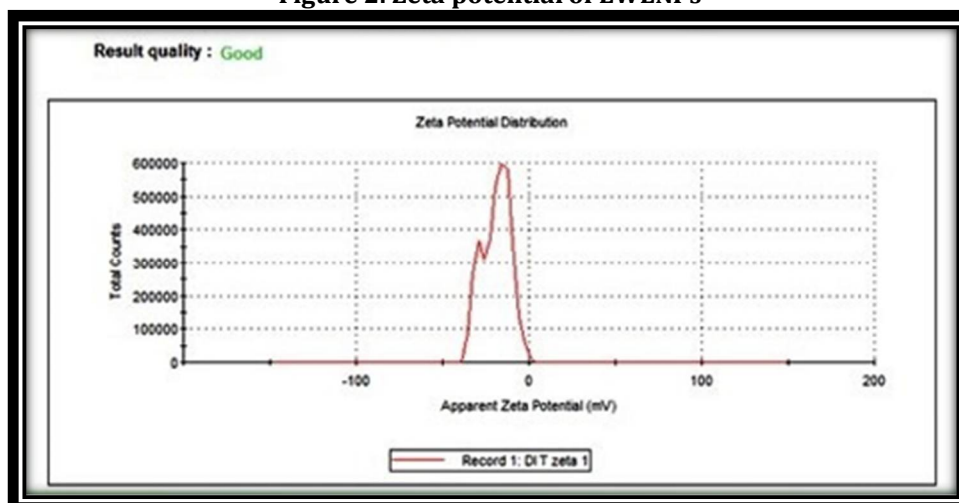


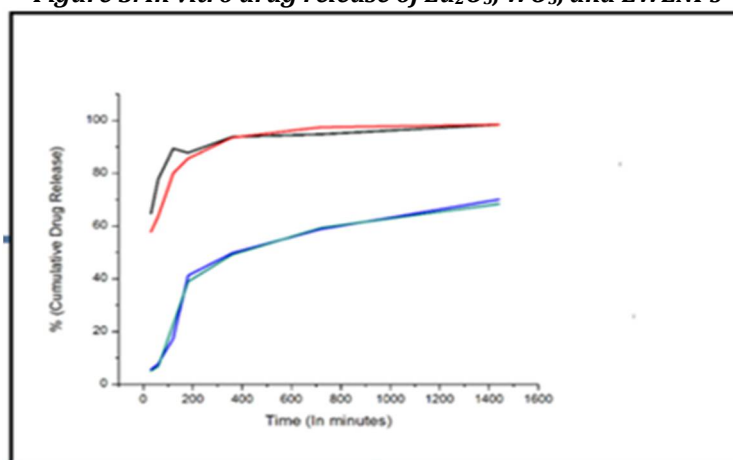
**Figure 2. Zeta potential of EWENPs**



### ***In vitro release profile of EWENPs***

The rate of discharge of  $\text{Eu}_2\text{O}_3$  and  $\text{WO}_3$  from nanoparticles is effectively mitigated by the polymeric matrix, which prevents rapid metabolism and destruction [24]. The in-vitro drug release percentages for  $\text{Eu}_2\text{O}_3$  and  $\text{WO}_3$  were found to be 79.88% and 81.12%, respectively, within a time frame of 3 hours. Nevertheless, it was noted that EWENPs containing 37.78% and 75.48%  $\text{Eu}_2\text{O}_3$  exhibited a prolonged release, with  $\text{WO}_3$  being released after 3 hours and 24 hours, respectively [25]. The release profile of EWENPs exhibited a prolonged and consistent release of  $\text{Eu}_2\text{O}_3$  and  $\text{WO}_3$  over time, owing to their inherent compatibility. The prolonged release of  $\text{Eu}_2\text{O}_3$  and  $\text{WO}_3$  particles is attributed to the formation of a cage-like thick and strong-walled dense matrix structure by Eudragit, as depicted in Figure 3.

**Figure 3. In vitro drug release of  $\text{Eu}_2\text{O}_3$ ,  $\text{WO}_3$ , and EWENPs**



### ***Percentage encapsulation efficiency***

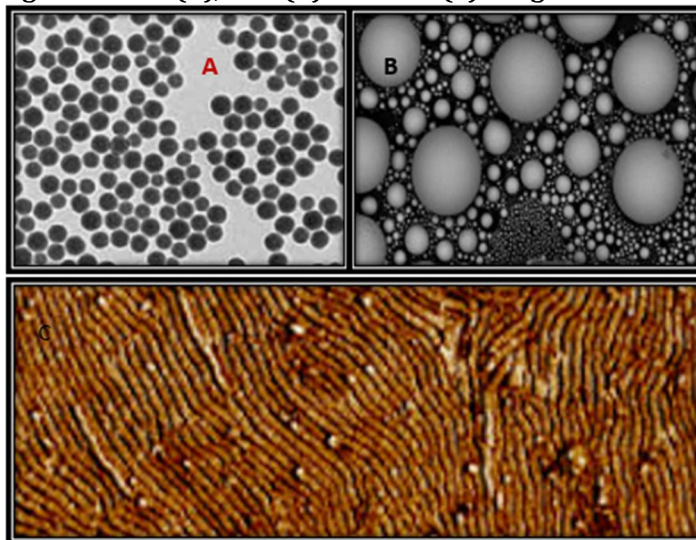
The efficacy of encapsulation is influenced by various factors, including the specific method used, the polarity of the molecule being encapsulated, and the molecular properties of the materials and media used in the creation of nanoparticles<sup>26</sup>. The encapsulation efficiency of EWENPs was found to be 89-92% correspondingly. The significant interaction between Eudragit and metallic oxides ( $\text{Eu}_2\text{O}_3$  and  $\text{WO}_3$ ) is attributed to the low dielectric constant of Eudragit, leading to an enhanced encapsulation efficiency of the medication within Eudragit.

### ***Morphological characterization of EWENPs by TEM, SEM, and AFM***

The drug release rate, solubility rate, and dissolution rate of a molecule/drug are influenced by the size, shape, and dimensions of nanoparticles. The migration of nanoparticles to different anatomical regions is influenced by their specific characteristics, including form, size, and dimensions<sup>27</sup>. The EWENPs exhibited a segregated nature and displayed a spherical morphology, with particle sizes ranging from 24 to 45 nm (Figure 4A). Variations in particle size were discovered through the use of particle size analysis (PSA) and transmission electron microscopy (TEM). The reason for this distinction is in the underlying concepts utilized by the PSA and TEM techniques. PSA relies on the ionic mobility of particles, while TEM operates

based on the analysis of particle dimensions inside an isolated environment. The spherical morphology of the nanoparticles was confirmed through analysis of scanning electron microscopy (SEM), as depicted in Figure 4B. Atomic Force Microscopy (AFM) provides a high level of resolution, wherein the intensity of the color corresponds to the height of the particle being observed. A diverse variety of particle sizes may be discerned, spanning from 2 nanometres to 3 millimeters (Figure 4C). Atomic Force Microscopy (AFM) exhibits a significantly reduced data acquisition time, about one-fourth, in comparison to Scanning Electron Microscopy (SEM) and Transmission Electron Microscopy (TEM) p<sup>28</sup>.

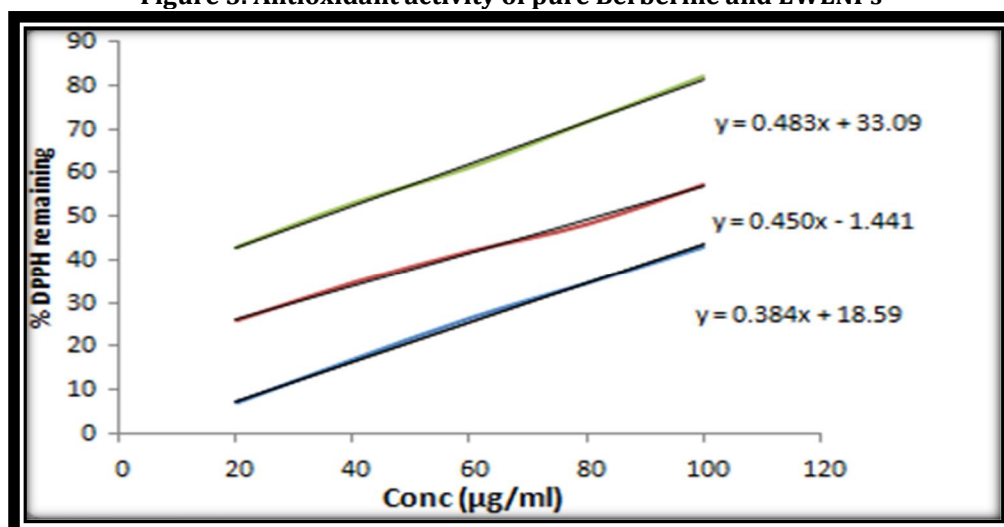
**Figure 4: TEM (A), SEM (B) and AFM (C) images of EWENPs**



#### **Anti-oxidant activity**

The DPPH technique is employed to quantify the antioxidant activity of encapsulated Eu<sub>2</sub>O<sub>3</sub> and WO<sub>3</sub> molecules<sup>29</sup>. The phenomenon of violet color disappearance is noticed upon the homogeneous combination of a DPPH solution with molecules of Eu<sub>2</sub>O<sub>3</sub> and WO<sub>3</sub>, which possess the ability to donate a hydrogen atom, thus exhibiting oxidizing properties. Eu<sub>2</sub>O<sub>3</sub> and WO<sub>3</sub> are widely recognized for their notable antioxidant properties. The mixture of Eu<sub>2</sub>O<sub>3</sub> and WO<sub>3</sub> was subjected to incubation with DPPH, resulting in a noticeable transformation of the hue from violet to pale yellow. Consequently, the absorbance band exhibited a decrease. The EWENPs showed a decreased level of inhibition of DPPH in comparison to the pure Eu<sub>2</sub>O<sub>3</sub> and WO<sub>3</sub>. This can be attributed to the gradual and prolonged release of the loaded Eu<sub>2</sub>O<sub>3</sub> and WO<sub>3</sub> particles within the EWENPs [32]. The encapsulation of Eu<sub>2</sub>O<sub>3</sub> and WO<sub>3</sub> by eudragit may be attributed to their nanometric size, which leads to a larger surface area [30]. This increased surface area is responsible for the observed enhancement in antioxidant activity when compared to the unencapsulated Eu<sub>2</sub>O<sub>3</sub> and WO<sub>3</sub>, as depicted in Figure 5.

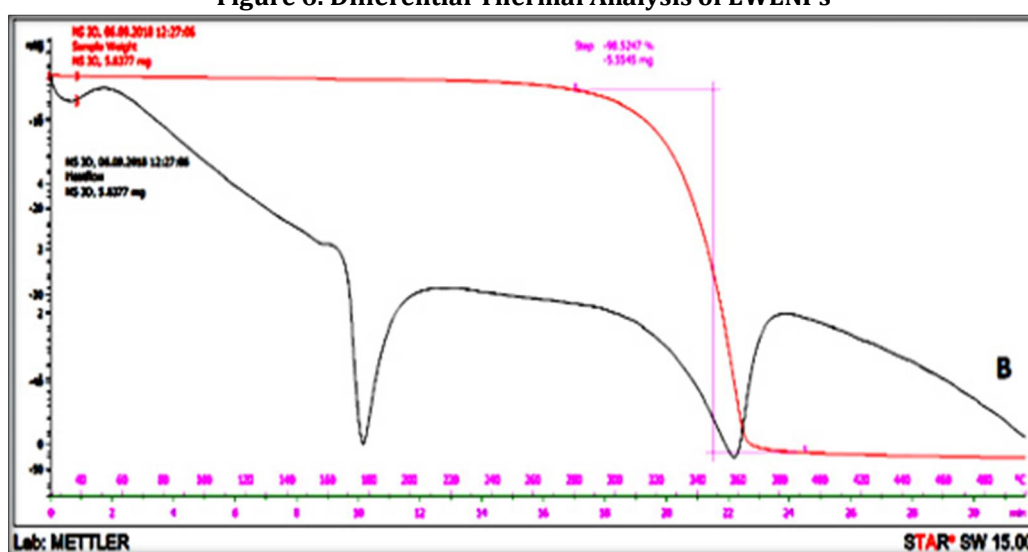
**Figure 5. Antioxidant activity of pure Berberine and EWENPs**



### DSC Analysis

Two endothermic peaks are observed in the DSC thermogram of free  $\text{Eu}_2\text{O}_3$  and  $\text{WO}_3$ . The initial endothermic peak occurs at a temperature of  $264^\circ\text{C}$ , exhibiting a relatively low intensity and is attributed to the presence of  $\text{Eu}_2\text{O}_3$  and  $\text{WO}_3$ . The presence of a strong high-intensity peak confirms the crystalline structure of the molecule. An investigation was conducted to examine the sharpness of all crests in the DSC diagram. The findings revealed that the nanoformulations exhibited an amorphous character, indicating that the drug in the nanoformulations was ideally in an amorphous state. The differential scanning calorimetry (DSC) thermogram of the  $\text{Eu}_2\text{O}_3$ - $\text{WO}_3$  nanocomposites (EWENPs) exhibits endothermic peaks with relatively low intensity, occurring at approximately  $400^\circ\text{C}$ . These peaks indicate the softening behavior of the  $\text{Eu}_2\text{O}_3$  and  $\text{WO}_3$  components. Furthermore, the disintegration process initiates at temperatures exceeding  $425^\circ\text{C}$ . The observed peak hump exhibits a relatively low power and lacks sharpness, therefore indicating its amorphous nature. The differential scanning calorimetry (DSC) thermogram of the polymeric nanoformulations exhibits two endothermic peaks. The first endothermic peak occurs at approximately  $170^\circ\text{C}$  and has a relatively modest intensity. The second endothermic peak was observed in proximity to a temperature of  $378^\circ\text{C}$ , suggesting that the onset of decomposition occurs subsequent to reaching a temperature of  $400^\circ\text{C}$ . The peak exhibits a relatively modest magnitude of force and lacks a clear sharpness, as indicated by the indistinct character observed in Figure 6.

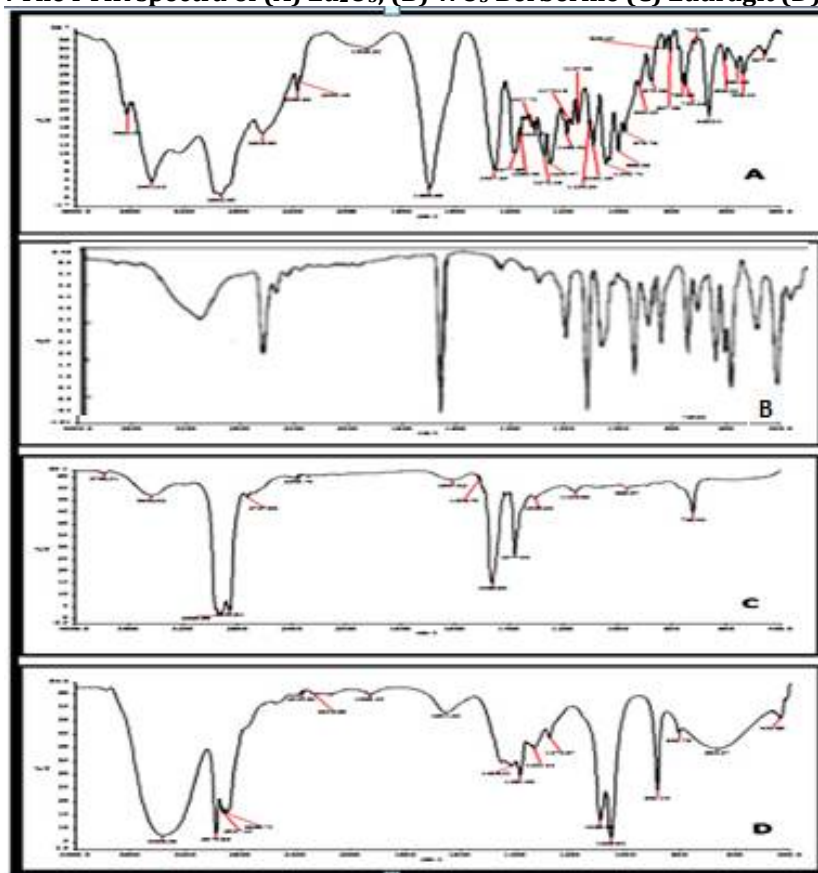
Figure 6. Differential Thermal Analysis of EWENPs



### FTIR Analysis of Drug Samples

FTIR spectroscopy was used to infer  $\text{Eu}_2\text{O}_3$ ,  $\text{WO}_3$ , and eudragit, interaction studies<sup>30</sup> as well as to confirm the loading of  $\text{Eu}_2\text{O}_3$ , and  $\text{WO}_3$  in EWENPs. FTIR spectrum of  $\text{Eu}_2\text{O}_3$ , and  $\text{WO}_3$  shows absorption bands at  $3157\text{ cm}^{-1}$  for  $-\text{OH}$  representing intermolecular H-bonding and  $2878\text{ cm}^{-1}$  &  $2324\text{ cm}^{-1}$  showing stretching bond (Fig 7). FTIR spectrum of eudragit is represented in Figure 7. Variation was found among wave numbers  $1548\text{ cm}^{-1}$  and  $848\text{ cm}^{-1}$  in EWENPs due to the formation of weak intermolecular bonds such as dipole-dipole interaction, and weak Van der Waals (depends upon molecular mass). Chitosan reveal characteristic peaks in the FTIR spectrum. Although peak intensity was decreased, bands were not shifted, signifying there is no chemical bond among  $\text{Eu}_2\text{O}_3$ ,  $\text{WO}_3$ , and eudragit. Figure 7 represents the FTIR spectrum of the physical combination of  $\text{Eu}_2\text{O}_3$ ,  $\text{WO}_3$ , and eudragit (EWENPs).

**Figure 7. The FTIR spectra of (A)  $\text{Eu}_2\text{O}_3$ , (B)  $\text{WO}_3$  Berberine (C) Eudragit (D) EWENPs**



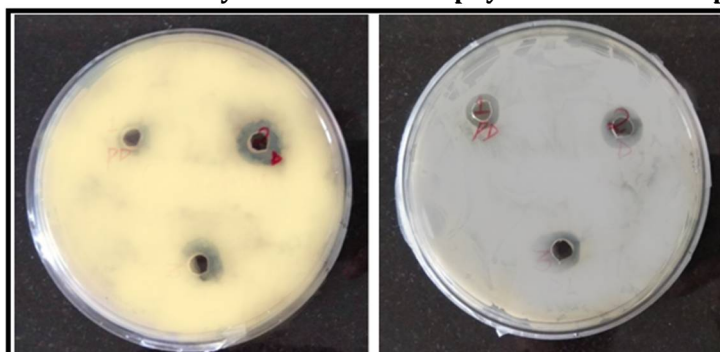
### **Anti-Inflammatory Activity**

The prevention of the lysis of the HRBC membrane was adopted as a measure of the anti-inflammatory activity of drugs. The results revealed that samples displayed a dose-dependent behavior of membrane stabilization i.e., as the concentration increased from 0.100 to 0.400 mg/ml; the percent protection was also increased. The maximum protection observed was 84.12 % from diclofenac sodium followed by  $\text{Eu}_2\text{O}_3$ , and  $\text{WO}_3$ , loaded eudragitnanoparticles (51.45%),  $\text{Eu}_2\text{O}_3$ , and  $\text{WO}_3$ , (22.67%) at 0.400 mg/ml, and blank nanoparticles (16.12 %). From the results, it can be concluded that  $\text{Eu}_2\text{O}_3$ , and  $\text{WO}_3$ , loaded eudragitnanoparticles showed significantly higher anti-inflammatory activity than pure  $\text{Eu}_2\text{O}_3$ , and  $\text{WO}_3$  and blank nanoparticles. Research findings have confirmed that  $\text{Eu}_2\text{O}_3$ , and  $\text{WO}_3$  in nanocomposite form have potent anti-inflammatory potency. Moreover, this  $\text{Eu}_2\text{O}_3$ , and  $\text{WO}_3$  can be considered as metallic oxides for the development of effective natural anti-inflammatory molecules [32].

### **Antibacterial Activity**

The antimicrobial potential of EWENPs was evaluated on Staphylococcus and Streptococcus strains (Figure 8). EWENPs have a potency to effectively kill as compared to  $\text{Eu}_2\text{O}_3$ , and  $\text{WO}_3$  as a control. The surface area of these nanoparticles is very high potentially raising their antibacterial activity [32, 33].

**Figure 8. The Antibacterial activity of EWENPs on Staphylococcus and Streptococcus strains**



## CONCLUSION

The development of nanotechnology has introduced a novel and highly effective approach to addressing a wide range of illnesses. Currently, a wide range of nanoformulations are being commercially promoted as effective strategies for combating bacterial infections. In this study, we examine the in vitro release rate, in vitro antioxidant capacity, and antibacterial effects of polymeric nanoformulations containing  $\text{Eu}_2\text{O}_3$  and  $\text{WO}_3$ -loaded eudragit nanoparticles. Both qualitative and quantitative methods are employed to explore these parameters. The utilization of chitosan polymer as a nanocarrier is attributed to its notable attributes, including its high safety profile, biocompatibility and biodegradability, antibacterial properties, and natural antioxidant activity. Moreover, it is worth noting that chitosan has been officially recognized as safe (GRAS) by the Food and Drug Administration for both human consumption and other applications. Experimental manipulation of polymer concentration resulted in alterations in both the size of nanoformulations and the efficacy of drug entrapment.  $\text{Eu}_2\text{O}_3$  and  $\text{WO}_3$  are molecules with anti-inflammatory and antibacterial properties. These molecules have the potential to be used in novel nanoformulations as effective excipients. This can lead to improved water solubility, bioavailability, and therapeutic efficacy against various disorders. The inclusion of surfactant molecules facilitates the penetration of  $\text{Eu}_2\text{O}_3$  and  $\text{WO}_3$  into nanoparticles, hence enabling the production of polymeric nanopatforms for effective drug delivery. The utilization of a novel polymeric nanocarrier containing  $\text{Eu}_2\text{O}_3$  and  $\text{WO}_3$ -loaded Eudragit nanoparticles shows potential as a viable approach to mitigate the presence of free radicals, which are known to contribute to the development of various types of cancer. This innovative nanocarrier has significant promise for future preclinical and clinical trials.

## REFERENCES

1. Sethi, N., Bhardwaj, P., Kumar, S., & Dilbaghi, N. (2019). Development and Evaluation of Ursolic Acid Co-Delivered Tamoxifen Loaded Dammar Gum Nanoparticles to Combat Cancer. *Advanced Science, Engineering and Medicine*, 11(11), 1115-1124.
2. Sethi, N., Bhardwaj, P., Kumar, S., & Dilbaghi, N. (2019). Development and Evaluation of Ursolic Acid Loaded Eudragit-E Nanocarrier For Cancer Therapy. *International Journal of Pharmaceutical Research* (09752366), 11(2).
3. Saini, A., Budania, L. S., Berwal, A., & Sethi, S. K. N. (2023). Screening of the Anticancer Potential of Lycopene-Loaded Nanoliposomes. *Tuijin Jishu/Journal of Propulsion Technology*, 44(4), 1372-1383.
4. Duan, G., Chen, L., Jing, Z., De Luna, P., Wen, L., Zhang, L., ... & Zhou, R. (2019). Robust antibacterial activity of tungsten oxide ( $\text{WO}_3$ -x) nanodots. *Chemical research in toxicology*, 32(7), 1357-1366.
5. Thakral, S., Thakral, N. K., & Majumdar, D. K. (2013). Eudragit®: a technology evaluation. *Expert opinion on drug delivery*, 10(1), 131-149.
6. Arshad, M., Ehtisham-ul-Haque, S., Bilal, M., Ahmad, N., Ahmad, A., Abbas, M., & Iqbal, M. (2020). Synthesis and characterization of Zn doped  $\text{WO}_3$  nanoparticles: photocatalytic, antifungal and antibacterial activities evaluation. *Materials Research Express*, 7(1), 015407.
7. Ahmed, B., Ojha, A. K., Singh, A., Hirsch, F., Fischer, I., Patrice, D., & Materny, A. (2018). Well-controlled in-situ growth of 2D  $\text{WO}_3$  rectangular sheets on reduced graphene oxide with strong photocatalytic and antibacterial properties. *Journal of hazardous materials*, 347, 266-278.
8. Nikam, V. K., Kotade, K. B., Gaware, V. M., Dolas, R. T., Dhamak, K., Somwanshi, S., & Kashid, V. (2011). Eudragit a versatile polymer: a review. *Pharmacologyonline*, 1(5), 152-164.
9. Zhang, J., Liu, X., Wang, X., Mu, L., Yuan, M., Liu, B., & Shi, H. (2018). Carbon dots-decorated  $\text{Na}_2\text{WO}_4$  composite with  $\text{WO}_3$  for highly efficient photocatalytic antibacterial activity. *Journal of hazardous materials*, 359, 1-8.
10. Patra, C. N., Priya, R., Swain, S., Jena, G. K., Panigrahi, K. C., & Ghose, D. (2017). Pharmaceutical significance of Eudragit: A review. *Future Journal of Pharmaceutical Sciences*, 3(1), 33-45.
11. Kaura, S., Parle, M., Insa, R., Yadav, B. S., & Sethi, N. (2022). Neuroprotective effect of goat milk. *Small Ruminant Research*, 214, 106748.
12. Nurbaisyatul, E. S., Azhan, H., Ibrahim, N., & Saipuddin, S. F. (2021). Structural and superconducting properties of low-density Bi (Pb)-2223 superconductor: Effect of  $\text{Eu}_2\text{O}_3$  nanoparticles addition. *Cryogenics*, 119, 103353.
13. Irshad, K. A., NV, C. S., Ravindran, T. R., Srihari, V., & Pandey, K. K. (2017). X-ray diffraction and Raman studies on Ho:  $\text{Eu}_2\text{O}_3$ . *Journal of Molecular Structure*, 1128, 325-329.
14. Moustafine, R. I., Zaharov, I. M., & Kemenova, V. A. (2006). Physicochemical characterization and drug release properties of Eudragit® E PO/Eudragit® L interpolyelectrolyte complexes. 100-55. *European Journal of Pharmaceutics and Biopharmaceutics*, 63(1), 26-36.
15. Vivek, V., Sethi, N., & Kaura, S. (2022). Green synthesis and evaluation of antibacterial activity of zinc nanoparticles from *Calotropis procera* leaves. *The Pharma Innovation Journal* 2022; 11(10): 1551-1554
16. Hajipour, M. J., Fromm, K. M., Ashkarran, A. A., de Aberasturi, D. J., de Larramendi, I. R., Rojo, T., & Mahmoudi, M. (2012). Antibacterial properties of nanoparticles. *Trends in biotechnology*, 30(10), 499-511
17. Sethi, N., Kaura, S., Dilbaghi, N., Parle, M., & Pal, M. (2014). Garlic: A pungent wonder from nature. *International research journal of pharmacy*, 5(7), 523-529.



18. Kilic, G., Issa, S. A., Ilik, E., Kilicoglu, O., & Tekin, H. O. (2021). A journey for exploration of Eu<sub>2</sub>O<sub>3</sub> reinforcement effect on zinc-borate glasses: Synthesis, optical, physical and nuclear radiation shielding properties. *Ceramics International*, 47(2), 2572-2583.
19. Milind, P., Sushila, K., & Neeraj, S. (2013). Understanding gout beyond doubt. *International Research Journal of Pharmacy*, 4(9), 25-34.
20. Hakimi-Tehrani, M. J., Hassanzadeh-Tabrizi, S. A., Koupaee, N., Saffar, A., & Rafiei, M. (2023). Synthesis of Z-scheme g-C<sub>3</sub>N<sub>4</sub>/WO<sub>3</sub> nano-photocatalyst with superior antibacterial characteristics for wastewater treatment. *Journal of Sol-Gel Science and Technology*, 105(1), 212-219.
21. Shubha, J. P., Savitha, H. S., Adil, S. F., Khan, M., Hatshan, M. R., Kavalli, K., & Shaik, B. (2021). Straightforward Synthesis of Mn<sub>3</sub>O<sub>4</sub>/ZnO/Eu<sub>2</sub>O<sub>3</sub>-Based Ternary Heterostructure Nano-Photocatalyst and Its Application for the Photodegradation of Methyl Orange and Methylene Blue Dyes. *Molecules*, 26(15), 4661.
22. Silver, L. L. (2011). Challenges of antibacterial discovery. *Clinical microbiology reviews*, 24(1), 71-109.
23. Murillo-Sierra, J. C., Hernández-Ramírez, A., Hinojosa-Reyes, L., & Guzmán-Mar, J. L. (2021). A review on the development of visible light-responsive WO<sub>3</sub>-based photocatalysts for environmental applications. *Chemical engineering journal advances*, 5, 100070.
24. Batalu, D., Stanciuc, A. M., Moldovan, L., Aldica, G., & Badica, P. (2014). Evaluation of pristine and Eu<sub>2</sub>O<sub>3</sub>-added MgB<sub>2</sub> ceramics for medical applications: Hardness, corrosion resistance, cytotoxicity and antibacterial activity. *Materials Science and Engineering: C*, 42, 350-361.
25. Wang, Q., Wang, H., Zhang, T., Hu, Z., Xia, L., Li, L., ... & Jiang, S. (2021). Antibacterial activity of polyvinyl alcohol/WO<sub>3</sub> films assisted by near-infrared light and its application in freshness monitoring. *Journal of Agricultural and Food Chemistry*, 69(3), 1068-1078.
26. Suman, J., Neeraj, S., Rahul, J., & Sushila, K. (2014). Microbial synthesis of silver nanoparticles by *Actinotalea* sp. MTCC 10637. *American Journal of Phytomedicine and Clinical Therapeutics*, 2, 1016-23.
27. Yang, X., Ning, G., & Lin, Y. (2007). Preparation of Eu (OH)<sub>3</sub> and Eu<sub>2</sub>O<sub>3</sub> nanorods through a simple method. *Chemistry letters*, 36(3), 468-469.
28. Devaraja, C., & Gowda, G. J. (2022). DC conductivity of heavy metal oxide (Bi<sub>2</sub>O<sub>3</sub>) boro-tellurite glasses: Effect of Eu<sub>2</sub>O<sub>3</sub>. *Journal of Metals, Materials and Minerals*, 32(2), 77-82.
29. Wang, Q., Wang, H., Zhang, T., Hu, Z., Xia, L., Li, L., ... & Jiang, S. (2021). Antibacterial activity of polyvinyl alcohol/WO<sub>3</sub> films assisted by near-infrared light and its application in freshness monitoring. *Journal of Agricultural and Food Chemistry*, 69(3), 1068-1078.
30. Chatterjee, M., Mondal, M., Sukul, T., Ghosh, K., & Pradhan, S. K. (2023). First-rate photocatalytic degradation of wastewater pollutants and antibacterial activities and H<sub>2</sub> evolution of hierarchical WO<sub>3</sub> embedded BiOCl/g-C<sub>3</sub>N<sub>4</sub> nanocomposites. *Journal of Industrial and Engineering Chemistry*, 127, 390-405.
31. Ashoka, N. B., Swamy, B. K., Jayadevappa, H., & Sharma, S. C. (2020). Simultaneous electroanalysis of dopamine, paracetamol and folic acid using TiO<sub>2</sub>-WO<sub>3</sub> nanoparticle modified carbon paste electrode. *Journal of Electroanalytical Chemistry*, 859, 113819.
32. Morales, W., Cason, M., Aina, O., de Tacconi, N. R., & Rajeshwar, K. (2008). Combustion synthesis and characterization of nanocrystalline WO<sub>3</sub>. *Journal of the American Chemical Society*, 130(20), 6318-6319.
33. Wang, F., Di Valentin, C., & Pacchioni, G. (2011). Electronic and structural properties of WO<sub>3</sub>: A systematic hybrid DFT study. *The Journal of Physical Chemistry C*, 115(16), 8345-8353.

#### CITATION OF THIS ARTICLE

Geeta, Pallavi Bhardwaj and Sunil K. Jangra. Biological activity of Eudragit loaded Eu<sub>2</sub>O<sub>3</sub>, and WO<sub>3</sub> nanocomposites against *Staphylococcus* and *Streptococcus* strain. *Bull. Env. Pharmacol. Life Sci., Spl Issue [2]: 2023: 578-586.*